Adaptive Non-singular Terminal Sliding Mode Control for an Unmanned Underwater Vehicle: Real-time Experiments

Miguel Angel Garcia Rangel, Adrian Manzanilla, Angel Eduardo Zamora Suarez, Filiberto Muñoz, Sergio Salazar, Rogelio Lozano

Adaptive Non-singular Terminal Sliding Mode Control for an Unmanned Underwater Vehicle: Real-time Experiments

Miguel Angel Garcia Rangel, Adrian Manzanilla, Angel Eduardo Zamora Suarez, Filiberto Muñoz*, Sergio Salazar, and Rogelio Lozano

Abstract: This research work focuses on the design of a robust-adaptive control algorithm for a 4DOF Unmanned Underwater Vehicle (UUV). The proposed strategy is based in a Non-Singular Terminal Sliding Mode Control (NTSMC) with adaptive gains, where the proposed adaptation mechanism ensures that the gains remain bounded. In this control strategy a non-singular terminal sliding surface is proposed to obtain a faster convergence of the tracking errors. The NTSMC ensures Practical Finite-Time Stability for the closed-loop system as well as exhibits a chattering reduction. In order to demonstrate the satisfactory performance of the proposed controller, a set of experiments was performed with a Non-Singular Terminal Sliding Mode Controller and an Adaptive Non-Singular Terminal Sliding Mode Control (ANTSMC) in real time for trajectory tracking in the X-Y plane, the graphs showed that the ANTSMC converges faster to a smaller region and reduces oscillations.

Keywords: Non-singular terminal sliding mode controller, real-time experiments, unmanned underwater vehicle.

1. INTRODUCTION

In recent years, Unmanned Underwater Vehicles (UUV's) have been used in different activities, such as: civilian, military and research tasks [1, 2]. Among their main applications are inspection of coastal structures, oceanographic monitoring, hull 3D reconstruction, under-water structure mapping, geological sampling and deep sea archaeology [3]. Moreover, the underwater vehicles are used to obtain relevant data from the underwater environment, such as temperature, dissolved oxygen, pH and salinity [4]. During the execution of the after mentioned undersea missions, underwater vehicles are expected to conduct these tasks in an automated way without the interaction of a human operator. Therefore, UUV's repre-sents an extensive field of study for many research groups around the world, due to the remarkable modelling dif-ficulties, such as highly non-linear terms, in addition to coupled dynamics, uncertainties and external disturbances in the UUV.

For a successful performance of the UUV's, it is nec-essary to have a control strategy that allows the vehicle to follow the desired trajectory [5], even under external disturbances. In this sense, the motion control problem for UUV's has received considerable attention due to its theoretical challenges. For example, classical controllers like: Proportional Integral Derivative (PID) [6], hierarchi-cal Proportional Derivative (PD) [7], robust PD [8]. As well as nonlinear and intelligent controllers, such as: back-stepping [9], sliding mode [10], backstepping with slid-ing modes [11], adaptive model predictive control [12], radial bases neural networks [13], adaptive fuzzy sliding mode [14], to name a few. However, the control of UUV's presents key challenges associated with complex dynam-ics, system uncertainties and environmental disturbances. These challenges are of notable interest and serve as a mo-tivation for this research work.

To cope with these challenges, sliding modes is a ro-bust control technique which provides robustness against unmodeled dynamics, insensitivity to parameter variations and disturbance rejection [15]. The main drawback of the sliding mode technique is the well-known chattering ef-fect [16]. However, there exist several ways to reduce or mitigate the chattering effect: using High Order Sliding Modes (HOSM) [16] or using a fast Terminal Sliding Mode (TSM)-type reaching law [17].

Miguel Angel Garcia Rangel, Adrian Manzanilla, Angel Eduardo Zamora Suarez, Filiberto Muñoz, Sergio Salazar, and Rogelio Lozano are with the Center for Research and Advanced Studies of the National Polytechnic Institute (CINVESTAV), Laboratory LAFMIA-UMI, Mexico (e-mails: {miguelgarciar, amanzanilla, angel.zamora, filiberto.munoz}@cinvestav.mx, sergio.salazar.cruz@gmail.com, rlozano@hds.utc.fr). Filiberto Muñoz is also with the National Council of Science and Technology (CONACYT), Mexico. Rogelio Lozano is also with Université de Technologie de Compiegne, Compiegne, France.
* Corresponding author.

The Super-Twisting (ST) is a HOSM algorithm that is commonly used for ro-bust control and observation, due to it reduces the chat-tering effect, respect to conventional sliding modes [18]. Moreover, for mechanical systems, the ST algorithm en-sures convergence to the sliding surface in finite-time, however the tracking errors converges to zero only exponentially [19–21].

Furthermore, to force the tracking errors to zero or a bounded set in finite-time, TSM and Non-Singular Terminal Sliding Mode controllers have been developed [17,22–24]. These control strategies have been applied to control marine vehicles. For example, a depth control for a remotely operated underwater vehicle using a NTSMC was developed in [25]. In [26], the trajectory tracking problem of an under-actuated unmanned underwater vehicle was solved using a finite-time control strategy. In this approach, the tracking errors globally converge to a neighborhood of the origin in finite-time. In [27] is developed a robust control strategy for the lateral motion of under-actuated AUV, a TSM controller guarantees the finite-time convergence of the tracking errors to zero. Moreover, a Non-Singular Terminal Sliding Mode (NSTSM) controller was developed in [28] for robust trajectory tracking of an AUV.

A well known issue with ST and NSTSM controllers is that the bounds of uncertainties and disturbances need to be know in advance. In order to overcome this drawback, adaptive strategies for sliding mode controllers have been developed [29]. Moreover, adaptive control automatically adjust the controller's gains in real-time in order to guarantees a successful performance when the parameters of the dynamic model are unknown. An adaptive sliding mode control is developed in [30], where adaptive sliding surfaces and adaptive control gains are designed. Adaptive versions of the super-twisting algorithm are developed in [31–33]. These versions reduce the chaterring effect, however only ensure asymptotic convergence of the tracking errors. An adaptive global terminal sliding mode controller is proposed in [34], where two adaptive laws are employed for the upper bound of uncertainties and disturbances.

In order to successfully control the dynamics of marine vehicles, adaptive sliding modes approaches have been proposed. In [32] is developed an adaptive gain generalized super-twisting algorithm for trajectory tracking of an AUV. In this manuscript experimental results are conducted for yaw and depth dynamics. In [35] an adaptive integral sliding mode for a class of UAVs is developed. To cope with parametric uncertainties and external disturbances, a neural neural network controller is added. An integral terminal sliding mode controller with adaptive compensation of uncertainties and disturbances is developed in [36] for an autonomous underwater vehicles.

In [37] an adaptive second-order fast non-singular terminal sliding mode is developed for tracking control of AUVs. The controller designed yields local exponential convergence of the position and attitude tracking errors to zero. An adaptive non-singular integral terminal sliding mode controller is developed in [38] for an AUV. The control strategy ensures that the velocity tracking errors locally converge to zero in finite time and after that the position tracking errors locally converge to zero exponentially.

The main contribution of this research work is the development of a Robust Adaptive Gain Non Singular Terminal Sliding Mode Controller. The proposed approach guarantees that the tracking errors converge to a bounded set in finite-time, even under unmodeled dynamics and external disturbances. In addition, a set of real-time experiments were conducted in X, Y, Z and yaw dynamic to demonstrate the performance of the proposed method.

From the comparison performed with [28, 36, 37] and [38], we can deduce that the controller proposed in this article has advantages, such as: a low computational cost since it does not depend of estimation of the dynamic parameters, presenting a rapid convergence to a small region [34] due to the adaptive gains of the controller, it does not present oscillations when the error is small. Moreover, the efficiency of the controller is validated by real-time experiments and obtain Root Mean Square Error, in contrast to the comparative articles where only simulation results are presented, the advantages found among the articles are summarized in the Table 1.

The remainder of the document is organized as follows: Section 2 describes the development of the dynamic model for the UUV. Section 3 presents the main contribution of this paper, which is the derivation of an adaptive-gain non-singular sliding mode control strategy for the UUV, as well as the stability analysis based on Lyapunov theory. Next, Section 4 demonstrates the controller performance through a series of experimental results for trajectory tracking tasks. Finally, Section 5 provides concluding remarks, as well as future research directions.

2. DYNAMIC MODEL OF UNDERWATER VEHICLES

The dynamic model for an underwater vehicle involves two coordinate frames: a body reference frame O_B and an inertial frame O_I, see Fig. 1. For this analysis, some of the main hydrodynamic effects of this type of vehicles are considered, in addition to considering restorative forces such as gravity and buoyancy. Considering the SNAME notation for underwater vehicles [39], the dynamic model in matrix form is written as [40]:

$$\begin{aligned} M\dot{\nu} + C(\nu)\nu + D(\nu)\nu + g(\eta) &= \tau + \omega, \\ \dot{\eta} &= J(\eta)\nu, \end{aligned} \tag{1}$$

Table 1. Comparative study between our research efforts and the existing literature closely related to our paper. In convergence speed of ✓is fast and ✓✓is very fast.

	Adaptive non-singular integral terminal sliding mode tracking control for autonomous underwater vehicles [38]	Adaptive second-order fast nonsingular terminal sliding mode tracking control for fully actuated autonomous underwater vehicles [37]	Non-singular terminal sliding mode control for robust trajectory tracking control of an autonomous underwater vehicle [28]	Double-loop integral termal sliding mode tracking control for UUV's with adaptive dynamic compensation of uncertainties and disturbances [36]	Our research.
Speed convergence of sliding surface:	✓	✓	✓	✓	✓✓
High computational cost:	yes	yes	no	no	no
Estimation of hydrodynamic parameters:	yes	yes	no	no	no
Experimental results in ψ and z	no	no	no	no	yes
Experimental results in x and y	no	no	no	no	yes

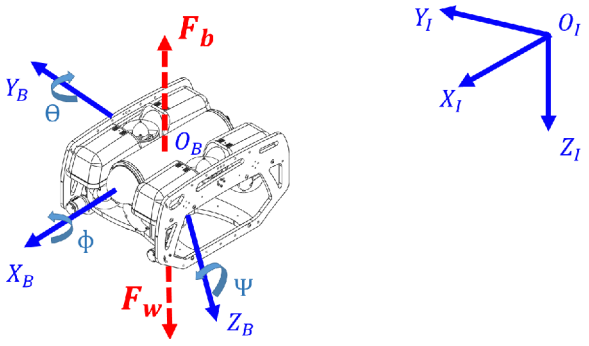

Fig. 1. Reference frames. Body fixed-frame O_B and earth-fixed reference frame O_I.

where M is the inertial matrix, $C(\nu)$ defines the Coriolis matrix, $D(\nu)$ denoting hydrodynamic damping matrix, $g(\eta)$ is the vector of hydrostatic forces, ω is the disturbance vector, $\tau = [X,Y,Z,K,M,N]^T \in \mathbb{R}^{6\times1}$ represents the vector of forces and moments in the body frame, $J(\eta)$ is the kinematic transformation between the body and the inertial frame, $\nu = [u,v,w,p,q,r]^T \in \mathbb{R}^{6\times1}$ describes the linear and angular velocities in the body frame, $\eta = [x,y,z,\phi,\theta,\psi]^T \in \mathbb{R}^{6\times1}$ denotes the vehicle's position and orientation in the inertial frame.

Due to the design of the vehicle, it is mechanically stable at the roll and pitch angles, that is $\phi \approx 0$, $\theta \approx 0$, see Fig. 1. Moreover, we assume that the vehicle operates at relative low speeds (i.e less than 2 m/s). For this vehicle, only the following reduced state vectors are taken into account: $\bar{\nu} = [u,v,w,r]^T$ and $\bar{\eta} = [x,y,z,\psi]^T$, likewise the reduced force vector $\bar{\tau} = [X,Y,Z,N]^T$. For the reduced 4-DOF dynamic equations, the matrices in the body frame are defined as

$$M = \text{diag}\left[m - X_{\dot{u}},\ m - Y_{\dot{v}},\ m - Z_{\dot{w}},\ I_{zz} - N_{\dot{r}}\right], \tag{2}$$

$$C(\bar{\nu}) = \begin{bmatrix} 0 & 0 & 0 & -(m-Y_{\dot{v}})v \\ 0 & 0 & 0 & (m-X_{\dot{u}})u \\ 0 & 0 & 0 & 0 \\ (m-Y_{\dot{v}})v & -(m-X_{\dot{u}})u & 0 & 0 \end{bmatrix}, \tag{3}$$

$$D(\bar{\nu}) = -\begin{bmatrix} X_u + X_{u_{|u|}}|u| & 0 & 0 \\ 0 & Y_v + Y_{v_{|v|}}|v| & 0 \\ 0 & 0 & Z_W + Z_{w_{|w|}}|w| \\ 0 & 0 & 0 \end{bmatrix} \begin{bmatrix} 0 \\ 0 \\ 0 \\ N_r + N_{r_{|r|}}|r| \end{bmatrix}, \tag{4}$$

$$g(\bar{\eta}) = [0,0,-(W-B),0]^T, \tag{5}$$

where m, W and B denote the mass, weight and buoyancy of the underwater vehicle, respectively. I_{zz} denotes the moment of inertia in the z-axis and N_r, $N_{r_{|r|}}$, Z_W, $Z_{w_{|w|}}$, Y_v, $Y_{v_{|v|}}$, X_u, $X_{u_{|u|}}$, $X_{\dot{u}}$, $Y_{\dot{v}}$, $Z_{\dot{w}}$ and $N_{\dot{r}}$ are the hydrodynamic parameters due to aggregate mass and vehicle shape.

The transformation between the body and inertial coordinate frames is given by

$$\ddot{\bar{\eta}} = \dot{\bar{J}}(\bar{\eta})\bar{J}(\bar{\eta})^{-1}\dot{\bar{\eta}} + \bar{J}(\bar{\eta})\dot{\bar{\nu}}, \tag{6}$$

with $\bar{J}(\bar{\eta})$ defined as

$$\bar{J}(\bar{\eta}) = \begin{bmatrix} c_\psi & -s_\psi & 0 & 0 \\ s_\psi & c_\psi & 0 & 0 \\ 0 & 0 & 1 & 0 \\ 0 & 0 & 0 & 1 \end{bmatrix}, \tag{7}$$

where $c_* = \cos(*)$ and $s_* = \sin(*)$.

From (6), the dynamic model of the underwater vehicle, expressed in the inertial frame O_I, is as follows:

$$\ddot{\bar{\eta}} = \bar{C}_\eta(\bar{\eta},\dot{\bar{\eta}})\dot{\bar{\eta}} + \bar{D}_\eta(\bar{\eta},\dot{\bar{\eta}})\dot{\bar{\eta}} + \bar{g}_\eta(\bar{\eta}) + \bar{\tau}_\eta, \tag{8}$$

where matrix $\bar{C}_\eta(\bar{\eta},\dot{\bar{\eta}})$, $\bar{D}_\eta(\bar{\eta},\dot{\bar{\eta}})$, $\bar{g}_\eta(\bar{\eta})$, $\bar{\tau}_\eta$. A detailed derivation of the dynamic model (8) is presented in Appendix A.

3. ADAPTIVE NON-SINGULAR SLIDING MODE CONTROL

In this section, the proposed control strategy for trajectory tracking of UUV's is presented. A non-singular terminal sliding mode controller is developed, where an adaptive mechanism for the controller's gain is introduced. The strategy proposed ensure that the tracking errors converge to a bounded region in finite-time. Some useful preliminaries are introduced below.

Definition 1: Assume a nonlinear system $\dot{\zeta} = f(\zeta,u)$, where ζ and u are the state and control signal. The solution is defines as Practical Finite-Time Stable (PFS) if for all ζ_0, there exist $\delta > 0$ and $T(\delta,\zeta_0)$ such that $\|\zeta(t)\| < \delta$ for all $t \geq t_o + T$. It is worth mentioning that PFS means finite-time boundedness.

Lemma 1 [41]**:** Consider the nonlinear system $\dot{\zeta} = f(\zeta,u)$. Assume that exists a continuous function $V(\zeta)$ and parameters $\lambda > 0$, $0 < \beta < 1$ and $0 < \omega < \infty$, such that

$$\dot{V}(\zeta) \leq -\lambda V^\beta(\zeta) + \omega. \tag{9}$$

Then, the system $\dot{\zeta} = f(\zeta,u)$ is PFS. Moreover, the system trajectory is bounded as

$$\lim_{a\to a_0} \zeta \in \left(V^\beta(\zeta) \leq \frac{\omega}{(1-a_0)\lambda}\right), \tag{10}$$

in finite time $t \leq T$ given by

$$T \leq \frac{V^{1-\beta}(\zeta_0)}{\lambda a_0(1-\beta)}, \quad 0 < a_0 < 1. \tag{11}$$

3.1. Control problem formulation

Consider a second-order dynamical system

$$\begin{aligned} \dot{\chi}_1 &= \chi_2, \\ \dot{\chi}_2 &= f(\chi_1,\chi_2) + g(\chi_1,\chi_2)u + \xi(\chi_1,\chi_2,t), \end{aligned} \tag{12}$$

where χ_1, χ_2 are the state variables, $f(\cdot)$, $g(\cdot)$ are nonlinear functions with $g(\cdot)^{-1} \neq 0$, u is the control input and $\xi(\cdot)$ is a bounded lumped disturbance. Moreover, disturbance $\xi(\cdot)$ satisfies $|\xi(\cdot)| \leq \xi^+$, with ξ^+ a positive constant. Let us define the tracking errors $e_1 = \chi_1 - \chi_{1_d}$ and $e_2 = \chi_2 - \chi_{2_d}$, where χ_{1_d} and χ_{2_d} denote the reference signals. The problem is to design a sliding mode controller that the tracking errors converges to a bound region in finite-time despite the presence of lumped disturbances.

Remark 1: Classical linear sliding surface has been used for a long time. Nowadays, it is widely used in Super Twisting sliding mode controllers [20, 32]. In this approach the surface is designed as

$$s = e_2 + ce, \quad c > 0. \tag{13}$$

In comparison with the conventional linear sliding surface, the control strategy developed in this research work has a faster convergence, enhanced with finite-time properties.

3.2. Control scheme design

Based on [17], an adaptive version for a Non-singular sliding mode controller for the trajectory tracking problem of an AUV is developed. The sliding surface employed is given by [22]

$$s = e_1 + \beta_1 \text{sig}^{\gamma_1} e_1 + \beta_2 \text{sig}^{\gamma_2} e_2, \tag{14}$$

where $\beta_1 > 0$, $\beta_2 > 0$, $1 < \gamma_2 < 2$, and $\gamma_1 > \gamma_2$. The notation $\text{sig}^\gamma a$ denotes $\text{sig}^\gamma a := |a|^\gamma \text{sign}(a)$, where $\text{sign}(\cdot)$ represents the sign function.

Theorem 1: Consider the dynamic system given by (12) and the non-linear sliding surface defined in (14). If the adaptive non-singular sliding mode control strategy is designed as

$$\begin{aligned} u = -\frac{1}{g(\chi_1,\chi_2)}\Bigg[&\frac{1}{\beta_2\gamma_2}\text{sig}^{2-\gamma_2}e_2 \cdot \left(1 + \beta_1\gamma_1|e_1|^{\gamma_1-1}\right) \\ &+ f(\chi_1,\chi_2) + \hat{k}_1 \text{sig}^\kappa s + \hat{k}_2 s - \dot{\chi}_{2_d}\Bigg], \end{aligned} \tag{15}$$

whit $0 < \kappa < 1$, and the adaptive gains $\hat{k}_1$ and $\hat{k}_2$ are updated [42] as

$$\dot{\hat{k}}_1 = \begin{cases} -\sigma_1, & \text{if } \hat{k}_1 > k_{1_{\max}} \\ -\sigma_2, & \text{if } k_{1_{\min}} < \hat{k}_1 < k_{1_{\max}} \text{ and } |s| < \Delta_s \\ \sigma_1, & \text{if } \hat{k}_1 \leq k_{1_{\min}} \text{ or } k_{1_{\min}} < \hat{k}_1 < k_{1_{\max}}, \\ & \text{and } |s| > \Delta_s, \end{cases} \tag{16}$$

$$\hat{k}_2 = \sigma_3 \hat{k}_1, \tag{17}$$

where σ_1, σ_2, σ_3, Δ_s, and $k_{1_{\max}} > k_{1_{\min}}$ are positive constants. Then, there exists a finite-time $t_F > 0$ such that the system trajectory will converge to the set defined by

$$|s| \leq \Omega = \min\{\Omega_1,\Omega_2\}, \tag{18}$$

$$\Omega_1 = \left(\frac{\omega_1}{(1-\theta)\alpha_{01}}\right), \tag{19}$$

$$\Omega_2 = \left(\frac{\omega_2}{(1-\theta)\,\alpha_{02}} \right)^{1/2}, \tag{20}$$

where $0 < \theta < 1$, and parameters ω_1, ω_2, α_{01} and α_{02} are defined below. Moreover, the tracking error e_1 and e_2 converge to the following regions

$$\begin{aligned} &|e_1| \leq 2\Omega, \\ &|e_2| \leq \left(\beta_2^{-1}\Omega\right)^{1/\gamma_2}, \end{aligned} \tag{21}$$

in finite-time.

Proof: Consider the Lyapunov function candidate as

$$V = \frac{1}{2}s^2 + \frac{1}{2}\tilde{k}_1^2 + \frac{1}{2}\tilde{k}_2^2, \tag{22}$$

where $\tilde{k}_1^2 = \hat{k}_1 - k_1$ and $\tilde{k}_2^2 = \hat{k}_2 - k_2$. Notice that the variables k_1 and k_2 are arbitrary constants used for stability analysis purposes. That is to say, k_1 and k_2 will not be employed in the control strategy. The time derivative of (22) along system (12) is given as

$$\begin{aligned} \dot{V} =& s\Big[e_2 + \beta_1\gamma_1|e_1|^{\gamma_1-1}e_2 + \beta_2\gamma_2|e_2|^{\gamma_2-1}\big(f(\chi_1,\chi_2) \\ &+ g(\chi_1,\chi_2)\,u + \xi(\chi_1,\chi_2,t) - \dot{\chi}_{2_d}\big)\Big] \\ &+ \tilde{k}_1\dot{\tilde{k}}_1 + \tilde{k}_2\dot{\tilde{k}}_2. \end{aligned} \tag{23}$$

Substituting the control law (15), we obtain

$$\begin{aligned} \dot{V} =& -\rho\left(\hat{k}_1|s|^{\kappa+1} + \hat{k}_2|s|^2 + s\xi(\chi_1,\chi_2,t)\right) \\ &+ \tilde{k}_1\dot{\tilde{k}}_1 + \tilde{k}_2\dot{\tilde{k}}_2, \end{aligned} \tag{24}$$

where $\rho = \beta_2\gamma_2|e_2|^{\gamma_2-1}$. From the fact that the disturbances is bounded and $0 < \kappa < 1$, we obtain

$$\dot{V} \leq -\rho\hat{k}_1|s| - \rho\hat{k}_2|s|^2 + \rho\xi^+|s| + \tilde{k}_1\dot{\tilde{k}}_1 + \tilde{k}_2\dot{\tilde{k}}_2. \tag{25}$$

The adaptive gain $\hat{k}_1$ is contained in the set $[k_{1_{\min}}, k_{1_{\max}}]$. Then from (25) we obtain

$$\dot{V} \leq -\rho|s|\left(k_{1_{\min}} - \xi^+\right) - \rho\hat{k}_2|s|^2 + \tilde{k}_1\dot{\tilde{k}}_1 + \tilde{k}_2\dot{\tilde{k}}_2. \tag{26}$$

If $k_{1_{\min}}$ is chosen such that $k_{1_{\min}} > \xi^+$, and $\underline{\hat{k}}_1 = k_{1_{\min}} - \xi^+$, then

$$\dot{V} \leq -\rho\underline{\hat{k}}_1|s| - \rho\hat{k}_2|s|^2 + \tilde{k}_1\dot{\tilde{k}}_1 + \tilde{k}_2\dot{\tilde{k}}_2. \tag{27}$$

From (27), the following two inequalities will hold

$$\dot{V} \leq -\rho\underline{\hat{k}}_1|s| + \tilde{k}_1\dot{\tilde{k}}_1 + \tilde{k}_2\dot{\tilde{k}}_2, \tag{28}$$

$$\dot{V} \leq -\rho\hat{k}_2|s|^2 + \tilde{k}_1\dot{\tilde{k}}_1 + \tilde{k}_2\dot{\tilde{k}}_2. \tag{29}$$

From inequality (28), we can obtain

$$\begin{aligned} \dot{V} \leq& -\frac{\alpha_{11}}{\sqrt{2}}|s| - \frac{\alpha_{21}}{\sqrt{2}}|\tilde{k}_1| - \frac{\alpha_{31}}{\sqrt{2}}|\tilde{k}_2| + \tilde{k}_1\dot{\tilde{k}}_1 + \tilde{k}_2\dot{\tilde{k}}_2 \\ &+ \frac{\alpha_{21}}{\sqrt{2}}|\tilde{k}_1| + \frac{\alpha_{31}}{\sqrt{2}}|\tilde{k}_2|, \end{aligned} \tag{30}$$

where $\alpha_{11} = \sqrt{2}\rho\underline{\hat{k}}_1$, $\alpha_{21} > 0$ and $\alpha_{31} > 0$. In view of $\left(b_1^2 + b_2^2 + b_3^2\right) \leq |b_1| + |b_2| + |b_3|$ is fulfilled for arbitrary real numbers b_1, b_2, b_3, the above inequality can be expressed as

$$V \leq -\alpha_{01}V^{1/2} + \omega_1, \tag{31}$$

where $\alpha_{01} = \min(\alpha_{11}, \alpha_{21}, \alpha_{3_1})$ and $\omega_1 = \tilde{k}_1\dot{\tilde{k}}_1 + \tilde{k}_2\dot{\tilde{k}}_2 + \frac{\alpha_{21}}{\sqrt{2}}|\tilde{k}_1| + \frac{\alpha_{31}}{\sqrt{2}}|\tilde{k}_2|$.
Thus, from Lemma 1 the system trajectory will converge in finite-time to the neighborhood of sliding surface $s = 0$ as

$$|s| \leq \left(\frac{\omega_1}{(1-\theta)\,\alpha_{01}} \right). \tag{32}$$

Applying a similar procedure to inequality (29) we obtain

$$|s| \leq \left(\frac{\omega_2}{(1-\theta)\,\alpha_{02}} \right)^{1/2}, \tag{33}$$

where $\omega_2 = \tilde{k}_1\dot{\tilde{k}}_1 + \tilde{k}_2\dot{\tilde{k}}_2 + \frac{\alpha_{22}}{\sqrt{2}}|\tilde{k}_1|^2 + \frac{\alpha_{32}}{\sqrt{2}}|\tilde{k}_2|^2$ with $\alpha_{22} > 0$, $\alpha_{32} > 0$; $\alpha_{02} = \min(\alpha_{12}, \alpha_{22}, \alpha_{32})$ with $\alpha_{12} = \sqrt{2}\rho\hat{k}_2$.

From (14), we can observe that the condition $e_2 = 0$ may inhibit the reachability to the region (18). To prove that this situation will not occur we proceed as follow. The control law (15) is replaced in the dynamic model (12) and setting $e_2 = 0$, we arrive to

$$\dot{e}_2 = -\left(\hat{k}_1 \mathrm{sig}^{\kappa}s + \hat{k}_2 s - \xi(\chi_1,\chi_2,t)\right). \tag{34}$$

When the sliding surface s is outside of the region Ω ($s \notin \Omega$), we can obtain

$$\dot{e}_2 = -\left(\left(\hat{k}_1 - \xi(\chi_1,\chi_2,t)\mathrm{sig}^{-\kappa}s\right)\mathrm{sig}^{\kappa}s + \hat{k}_2 s\right) \neq 0, \tag{35}$$

$$\dot{e}_2 = -\left(\hat{k}_1 \mathrm{sig}^{\kappa}s + \left(\hat{k}_2 - \xi(\chi_1,\chi_2,t)s^{-1}\right)s\right) \neq 0. \tag{36}$$

Notice that from previous equations we get $e_2 \neq 0$, which means that the system trajectory will no remain in the region $e_2 = 0$, $s \notin \Omega$. Therefore, the finite-time reachability of the sliding surface (14) is still guaranteed.

Combining (14) and (18) we obtain

$$s = e_2 + \beta_1 \mathrm{sig}^{\gamma_1}e_1 + \beta_2 \mathrm{sig}^{\gamma_2}e_2 <= \Omega, \tag{37}$$

which can be rewritten as

$$e_2 + \beta_1 \mathrm{sig}^{\gamma_1}e_1 + \left(\beta_2 - s\cdot\mathrm{sig}^{1/\gamma_2}e_2\right)\mathrm{sig}^{\gamma_2}e_2 = 0. \tag{38}$$

If $\beta_2 - s\cdot\mathrm{sig}^{1/\gamma_2}e_2 > 0$ is fulfill, inequality (38) remains as a TSM. Thus, the velocity tracking error will converge to the following region

$$|e_2| \leq |\beta_2^1 s|^{1/\gamma_2} \leq |\beta_2^1\Omega|^{1/\gamma_2}. \tag{39}$$

Combining (38) and (39) we obtain that the position tracking error will converge to the following bound

$$|e| = 2\Omega. \tag{40}$$

It is worth mentioning that the control signal (15) doesn't involve negative fractional power, thus it is non-singular.□

3.3. Control strategy for the 4DOF autonomous underwater vehicle

The control strategy for the UUV in surge, sway, heave and heading is based on the robust non-singular sliding mode controller developed in Subsection 3.2. From control signal (15), we have the following control signals

- Surge

$$X = -\frac{1}{g_x}\left[\frac{1}{\beta_{2_x}\gamma_{2_x}}\text{sig}^{2-\gamma_{2_x}} e_{2_x}\cdot\left(1+\beta_{1_x}\gamma_{1_x}|e_{1_x}|^{\gamma_{1_x}-1}\right)\right. \tag{41}$$

$$\left. + f_x + \hat{k}_{1_x}\text{sig}^{\kappa_x} s^x + \hat{k}_{2_x} s^x - x_{2_d}\right]. \tag{42}$$

- Sway

$$Y = -\frac{1}{g_y}\left[\frac{1}{\beta_{2_y}\gamma_{2_y}}\text{sig}^{2-\gamma_{2_y}} e_{2_y}\cdot\left(1+\beta_{1_y}\gamma_{1_y}|e_{1_y}|^{\gamma_{1_y}-1}\right)\right.$$

$$\left. + f_y + \hat{k}_{1_y}\text{sig}^{\kappa_y} s^y + \hat{k}_{2_y} s^y - y_{2_d}\right]. \tag{43}$$

- Heave

$$Z = -\frac{1}{g_z}\left[\frac{1}{\beta_{2_z}\gamma_{2_z}}\text{sig}^{2-\gamma_{2_z}} e_{2_z}\cdot\left(1+\beta_{1_z}\gamma_{1_z}|e_{1_z}|^{\gamma_{1_z}-1}\right)\right.$$

$$\left. + f_z + \hat{k}_{1_z}\text{sig}^{\kappa_z} s^z + \hat{k}_{2_z} s^z - z_{2_d}\right]. \tag{44}$$

- Heading

$$N = -\frac{1}{g_\psi}\left[\frac{1}{\beta_{2_\psi}\gamma_{2_\psi}}\text{sig}^{2-\gamma_{2_\psi}} e_{2_\psi}\cdot\left(1+\beta_{1_\psi}\gamma_{1_\psi}|e_{1_\psi}|^{\gamma_{1_\psi}-1}\right)\right.$$

$$\left. + f_\psi + \hat{k}_{1_\psi}\text{sig}^{\kappa_\psi} s^\psi + \hat{k}_{2_\psi} s^\psi - \psi_{2_d}\right]. \tag{45}$$

The functions f_x, f_y, f_z, f_ψ, g_x, g_y, g_z, g_ψ are given in Appendix A. The sliding surfaces s^x, s^y, s^z and s^ψ are defined accord to (14).

4. REAL-TIME EXPERIMENTS

In this section, a brief description of the UUV used to implement the control strategy developed is presented. As well as the description of the real-time experiments realized in surge, sway, heave and heading.

4.1. Description of the underwater vehicle

The BlueROV2 is the underwater vehicle used for the realization of real-time experiments, see Fig. 2. This vehicle is connected to a ground station through meta-operating system ROS (Robot Operating System), the power supply is by means of Li-Po batteries, which are in the vehicle. The ground terminal acquires the data of the robot's sensors such that the controller calculates the torque for the thrusters. The control algorithms are executed with a sampling period of 50 milliseconds. The vehicle's dimensions are $45.71 \times 33.81 \times 22.1$ cm with a weight of 11.5 Kg. This vehicle has the capacity to submerge up to 100 m. The known vehicle parameters are presented in Table 2.

The electronic structure of the BlueROV2 is illustrated in Fig. 3, where you can see that it uses a Pixhawk autopilot, which is connected to a Raspberry pi 3, which has a camera that can transmit video in real time through a Fathom-X Tether, which connects to the ground station.

The estimation of the current position and orientation of the UUV it is transmitted of the vehicle is by water linked API and BlueROV2, the submarine has a hydrophone that sends an acoustic pulse to four receiving beacons. The received acoustic signal is processed in a positioning com-

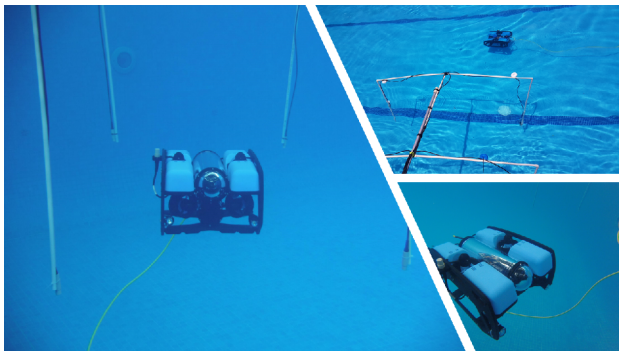

Fig. 2. This figure shows the system used to locate the BlueROV2, which consists of four hydrophones, a transmitter mounted on the vehicle and a ground station (master).

Table 2. Physical and dynamic parameters of the BlueROV2.

Param.	Value.	Param.	Value.	Param.	Value.
$\vec{W}$	$[0,0,176]^T$	$X_{\dot{u}}$	5.5	$Y_{\dot{v}}$	12.7
$\vec{r}_b$	$[0,0,-0.1]^T$	$Z_{\dot{w}}$	14.57	I_{xx}	0.16
$\vec{B}$	$[0,0,9.81m_f]^T$	I_{yy}	0.16	I_{zz}	0.16
$K_{\dot{p}}$	0.002	$M_{\dot{q}}$	0.002	$N_{\dot{r}}$	0.12
X_u	3.03	Y_v	3.21	Z_w	8.18
K_p	2	M_q	0.1	N_r	0.07
X_{u_c}	4.03	Y_{v_c}	6.21	Z_{w_c}	5.18
K_{p_c}	0.07	M_{q_c}	0.07	N_{r_c}	0.07

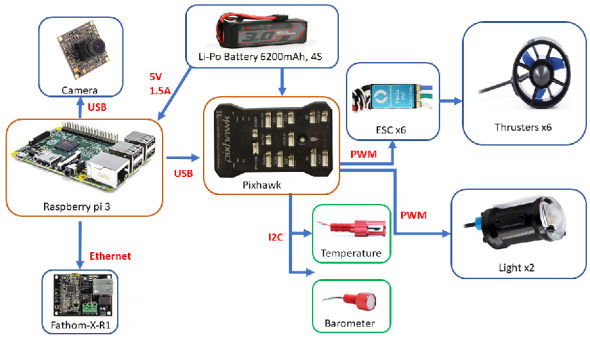

Fig. 3. BlueROV2 electronic elements diagram.

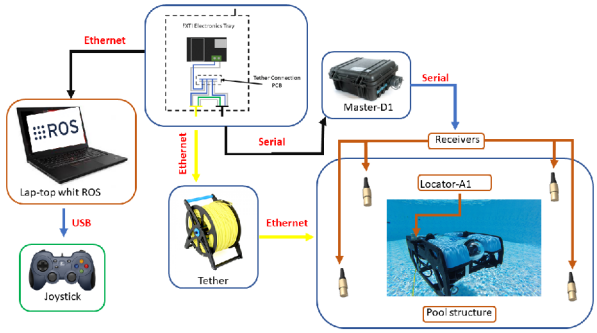

Fig. 4. This diagram shows the elements used, to perform the tests in a pool.

puter that calculates the time of arrival of the signal to each receiving beacon and using the data fusion of sensors, the robot position is triangulated. The range of the underwater GPS system is $200 \times 200 \times 100$ meters, its update rate is 4 Hz.

It is important to mention that the accuracy of the location system is affected by acoustic reflections, therefore, a second order low pass filter is implemented to attenuate background noise, for a better understanding you can see Fig. 4. The ground station is the Lenovo Thinkpad T430 notebook, equipped with Intel Core i5-3210M (3.1 GHz frequency), 8GB RAM memory, SSD hard drive under Linux Xenial 16.04 LTS operating system and ROS Kinetic. Such a computer was proposed for the autonomous control of the BlueROV2, to conduct all necessary calculations at the ground station, including: data (measurements) processing, autonomous control, etc.

4.2. Real-time experiments

In this section, the control strategy (15) developed in this research work was applied to control the surge, sway, depth and heading dynamics of the UUV. In order to show the outperformance of the strategy proposed, we conducted a comparative study, in the surge and sway dynamic, with the NSTSM controller presented in [28].

The parameters of the controller and the adaptive law

Algorithm 1: Procedure for the implementation of ANTSMC Controller by using BlueROV2, ROS and Water Linked GPS API

1: **Requiere:** Install mavros, bluerov-ros-pkg, Water Linked Underwater GPS API and all necessary dependencies.
2: Initialize the communication with the BlueROV2 vehicle by modifying the network configuration and selecting a valid IP.
3: Initialize the Water Linked GPS through the API.
4: Define a desired trajectory for the position and orientation of the BlueROV2 vehicle.
5: **while** No error **do**
6: Get the BlueROV2 orientations and positions from the IMU and the underwater GPS, respectively.
7: Calculate the control laws (41-44) for the BlueROV2 to reach trajectory in position (Surge, Sway and Heave) and orientation (Yaw).
8: Send the command to the thrusters of the vehicle based on the previous control laws.
9: **end while**
10: Close all communications.

Table 3. Controller gains and adaptive law parameters.

Parameters of the controller and adaptive laws		
$\beta_{x_1} = 4$	$\gamma_{x_2} = 1.1$	$k_{1_{x\min}} = 12.5$
$\beta_{x_2} = 5$	$\Delta_x = 3.5$	$\sigma_{x_1} = 0.2$
$\gamma_{x_1} = 1.3$	$k_{1_{x\max}} = 15$	$\sigma_{x_2} = 2$
$\beta_{y_1} = 8$	$\gamma_{y_2} = 1.1$	$k_{1_{y\min}} = 12.5$
$\beta_{y_2} = 7$	$\Delta_y = 3.5$	$\sigma_{y_1} = 0.2$
$\gamma_{y_1} = 1.3$	$k_{1_{y\max}} = 13$	$\sigma_{y_2} = 2$
$\beta_{z_1} = 150$	$\gamma_{z_2} = 1.1$	$k_{1_{z\min}} = 13$
$\beta_{z_2} = 50$	$\Delta_z = 3.5$	$\sigma_{z_1} = 1$
$\gamma_{z_1} = 1.2$	$k_{1_{z\max}} = 15$	$\sigma_{z_2} = 2$
$\beta_{\psi_1} = 5$	$\gamma_{\psi_2} = 1.05$	$k_{1_{\psi\min}} = 1.1$
$\beta_{\psi_2} = 6$	$\Delta_\psi = 10$	$\sigma_{\psi_1} = 0.25$
$\gamma_{\psi_1} = 1.5$	$k_{1_{\psi\max}} = 1.35$	$\sigma_{\psi_2} = 2$

were adjusted heuristically and are summarized in Table 3. Experimental tests are performed in a pool of dimensions $25 \times 20 \times 3$ m, four test scenarios are proposed. In three scenarios the same trajectory is used, in surge, sway and yaw angle. Algorithm 1 presents the steps to implement the algorithm to real-time experiments.

The desired route is carried out using the parametric equations given by:

$$\chi_{1d}(t) = \chi_f \left[10\left(\frac{t}{t_f}\right)^3 - 15\left(\frac{t}{t_f}\right)^4 + 6\left(\frac{t}{t_f}\right)^5 \right],$$
$$\chi_{2d}(t) = \chi_f \left[30\left(\frac{t^2}{t_f{}^3}\right) - 60\left(\frac{t^3}{t_f{}^4}\right) + 30\left(\frac{t^4}{t_f{}^5}\right) \right], \quad (46)$$

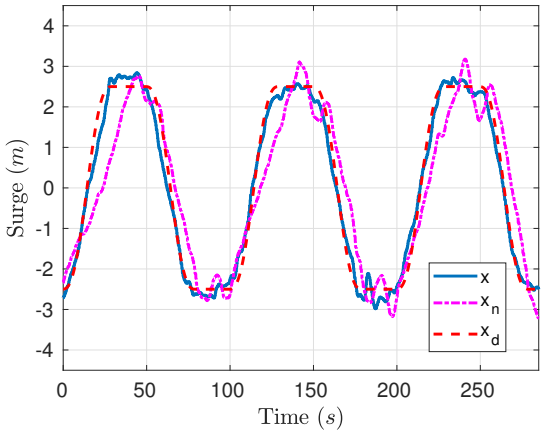

Fig. 5. Trajectory tracking in position x using acoustic localization. x_d desired (dashed red line), x trajectory with ANTSMC (solid blue line) and x_n trajectory with NSTSM controller (dashed point magenta line).

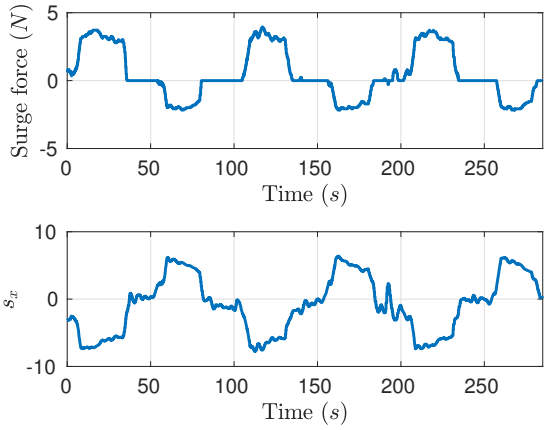

Fig. 6. Control input and sliding surface in surge controller for the ANTSMC.

where χ_f is the final position and t_f is the final route time.

In the first scenario, the comparative tests the trajectory tracking of the submarine vehicle on the x-axis is given by (46) with $\chi_f \pm 2.5$ and $t_f = 30$. The first comparative test is performed with the trajectory tracking on the x-axis, the results of UUV can be seen in Fig. 5. We can observed that the reference is reached in both cases, however, it is visible that the trajectory tracking error is smaller with the proposed controller.

The graphs of the evolution of the control input and the sliding surface for ANTSMC are shown in Fig. 6, note that there is an attenuation in the chattering effect and that the surface is maintained in a convergence region close to zero.

Moreover, in Fig. 7 we can see the response of the control input and the sliding surface for NSTSM controller,

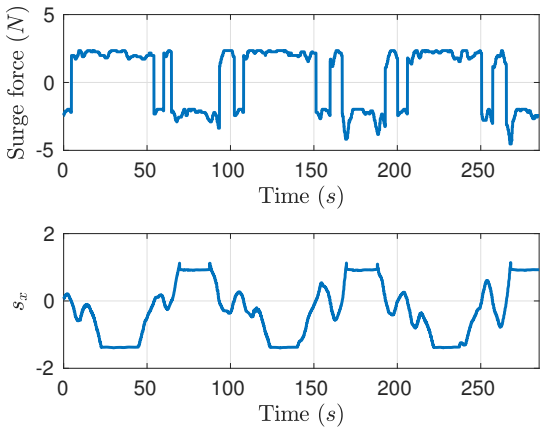

Fig. 7. Control input and sliding surface in surge controller using NSTSM controller.

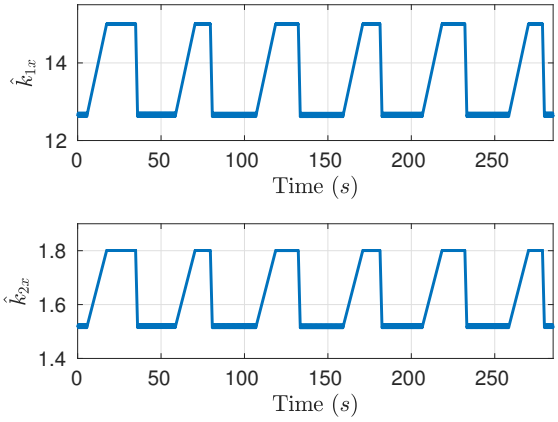

Fig. 8. Adaptive gains in surge controller.

notice that the sliding surface doesn't converge in a region close to zero. Finally, for the first scenario the evolution of the adaptation of the parameters $\hat{k}_{1x}$ and $\hat{k}_{2x}$ are presented in Fig. 8.

In the second scenario, trajectory tracking is performed on the y-axis using the reference proposed by (46) with the same conditions as scenario 1. As shown in Fig. 9, the behavior of the trajectory tracking performed is reported. We can appreciate that it is close to the reference in both cases but the trajectory tracking error on Sway with NSTSM controller is bigger that with the ANTSMC. We can observe that the reference is reached and it is visible that when it reaches the final position there is an overshoot using the NSTSM controller.

Fig. 10 shows that there was also attenuation in the chattering effect and that the control input is very small approximately only 10% of the force provided by the thrusters. Moreover, it can be seen that sliding surface being maintained in a region. On the other hand, in Fig. 11 the response of the control input and the evolution of the

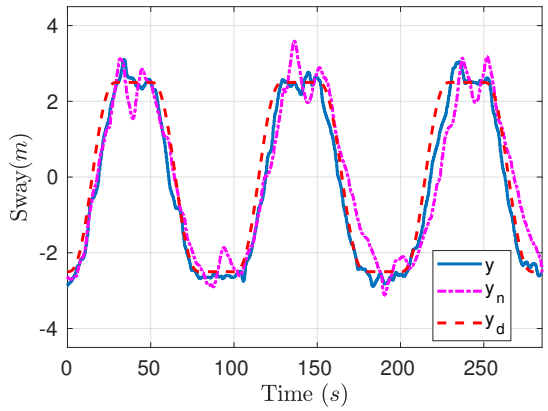

Fig. 9. Trajectory tracking in position y using acoustic localization. y_d desired (dashed red line), y trajectory with ANTSMC (solid blue line) and y_n trajectory with NSTSM controller (dashed point magenta line).

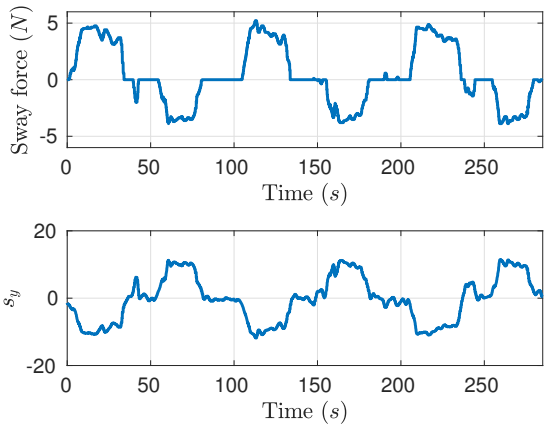

Fig. 10. Control input and sliding surface in sway controller, using the ANTSMC.

sliding surface of the NSTSM controller are displayed. We can observe that the sliding surface presents oscillations when it converges to a close region zero.

We can observe in Fig. 12 the temporal evolution of the adaptation of gains $\hat{k}_{1y}$ and $\hat{k}_{2y}$, it can be noted that the adaptive gains remain bounded. In the Table 4, we obtain the RMSE for each controller and conclude that the controller proposed in (15) is more efficient in both scenarios, i.e, the proposed controller has a very small tracking error.

The third scenario was followed by a sinusoidal reference in depth given by equations

$$z_{1d} = -1.4 + 1.2 * \sin\left(\frac{2\pi}{120}t\right),$$
$$z_{2d} = 1.2 * \frac{2\pi}{120} * \cos\left(\frac{2\pi}{120}t\right). \quad (47)$$

In Fig. 13, the results of the depth trajectory tracking are

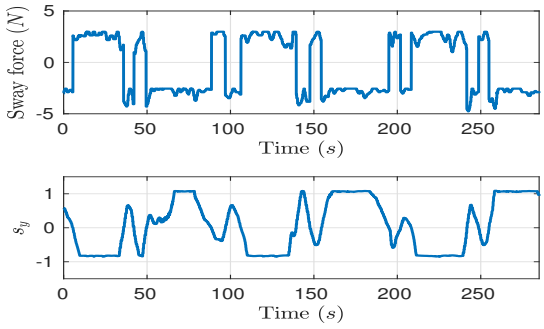

Fig. 11. Control input and sliding surface in sway controller, using the NSTSM controller.

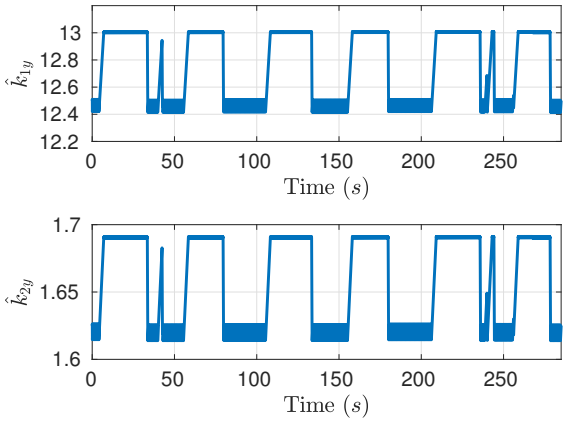

Fig. 12. Response of the adaptive gains in sway controller.

Table 4. Root Mean Square Error criterion for surge and sway controllers.

RMSE (m)		
NSTSM controller	x	0.2424
	y	0.1932
ANTSMC	x	0.1288
	y	0.0686

presented. Note that the reference signal is reached in a short time and that the tracking is quite satisfactory with almost no tracking error. Also, we can be seen in Fig. 14 the response of the control signal and the behavior of sliding surface from stay in a region very close to zero.

The evolution of the adaptive parameters k_{1z} and k_{2z} are shown in Fig. 15, note that both parameters remain at the lower limit because the sliding surface converges to a region near zero. Finally, in the fourth scenario the yaw trajectory tracking given by (46) was carried out with $\chi_f = 100$ and $t_f = 30$. The results of this experimental test are presented in Fig. 16, we can see that the desired orientation is reached along trajectory tracking.

The efficiency of the UUV trajectory tracking during

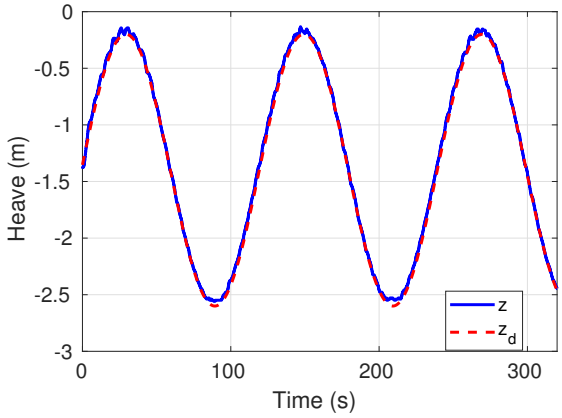

Fig. 13. Autonomous trajectory tracking in depth using the ANTSMC.

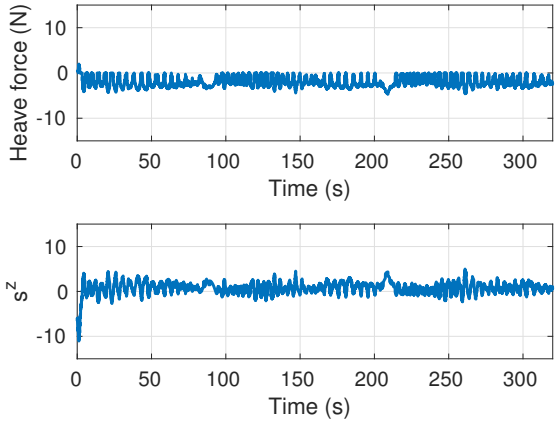

Fig. 14. Control input and sliding surface in heave controller, using the ANTSMC.

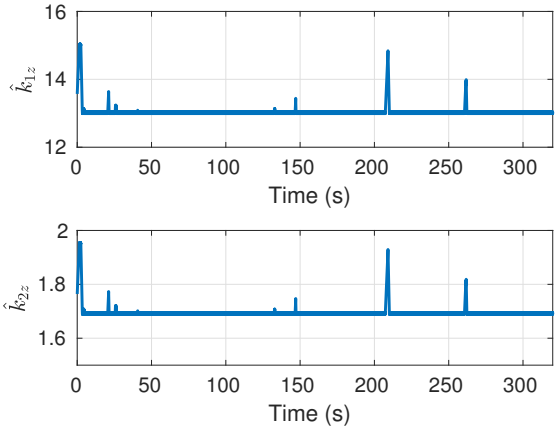

Fig. 15. Adaptive gains in heave controller.

the four scenarios can be seen in the following video: https://youtu.be/2DrcwiENBHI. We can observe the behavior of the robot during experimental tests and the accuracy of the trajectory tracking.

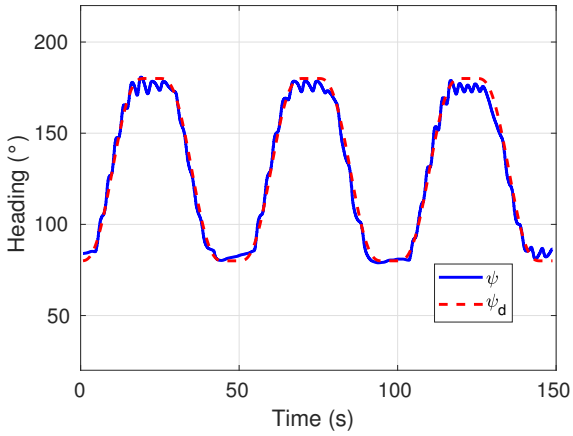

Fig. 16. Angular position, ψ is the yaw angle and ψ_d is the desired yaw angle, used NSTSM controller.

Remark 2: The adaptive controller's gains increasing and decreasing in a bounded region, which implies that the closed loop system remains stable. For the robust-adaptive control strategies developed in [29, 32], the controller gains keep increasing. If the initial tracking errors are large or in presence of external disturbances, these situations would give rise to large control signals, actuator saturation and even failures in the system.

5. CONCLUSION

In this research work, we developed and implemented an ANTSMC for the trajectory tracking of an UUV, moreover to perform a practical comparison with an NSTSM controller, in order of know the advantages that the proposed controller offers. The real-time experimental results obtained demonstrate the behavior of the closed loop system and the effectiveness of the proposed controller strategy. We conclude, based on the results obtained and the calculation of RMSE, that the strategy proposed is more efficient that NSTSM controller. In addition, the graphics of the behavior of adaptive parameters show the evolution of gains by decreasing or increasing its value in a bounded region, according to the magnitude of the sliding surface. Also, a significant reduction of the chattering effect in the control signal is observed. To further our research we will develop a disturbance observer that enable us to estimate external unknown disturbances. Furthermore, we will conduct sea-trial in more aggressive environments.

APPENDIX A

From (1) and (6), the dynamic model of the underwater vehicle, expressed in the inertial frame O_I, is given as

follows:

$$\begin{aligned}\ddot{\bar{\eta}} = &-\bar{M}^{-1}(\bar{\eta})\bar{C}(\bar{\eta},\dot{\bar{\eta}})\dot{\bar{\eta}} - \bar{M}^{-1}(\bar{\eta})\bar{D}(\bar{\eta},\dot{\bar{\eta}})\dot{\bar{\eta}} \\ &-\bar{M}^{-1}(\bar{\eta})\bar{g}(\bar{\eta}) + \bar{M}^{-1}(\bar{\eta})\bar{\tau}, \end{aligned} \tag{A.1}$$

where

$$\begin{aligned}\bar{M}(\bar{\eta}) &= M\bar{J}^{-1}(\bar{\eta}), \\ \bar{D}(\bar{\eta},\dot{\bar{\eta}}) &= D(\bar{J}(\bar{\eta})^{-1}\dot{\bar{\eta}})\bar{J}(\bar{\eta})^{-1}, \\ \bar{C}(\bar{\eta},\dot{\bar{\eta}}) &= -M\bar{J}^{-1}(\bar{\eta})\dot{\bar{J}}(\bar{\eta})\bar{J}^{-1}(\bar{\eta}) \\ &\quad + C(\bar{J}(\bar{\eta})^{-1}\dot{\bar{\eta}})\bar{J}(\bar{\eta})^{-1}. \end{aligned} \tag{A.2}$$

The matrices that represent the dynamic model in the inertial framework are defined as

$$\bar{M}(\bar{\eta}) = \begin{bmatrix} (m-X_{\dot{u}})c_\psi & (m-X_{\dot{u}})s_\psi & 0 & 0 \\ -(m-Y_{\dot{v}})s_\psi & (m-Y_{\dot{u}})c_\psi & 0 & 0 \\ 0 & 0 & m-Z_{\dot{w}} & 0 \\ 0 & 0 & 0 & I_{zz}-N_{\dot{r}} \end{bmatrix}. \tag{A.3}$$

Calculating the $\bar{C}(\bar{\eta},\dot{\bar{\eta}})$ matrix in terms of $\bar{\eta}$ and the vehicle's conditions we obtain

$$\bar{C}(\bar{\eta},\dot{\bar{\eta}}) = \begin{bmatrix} -(m-X_{\dot{u}})\dot{\psi}s_\psi & C_{12} & 0 & -C_{14} \\ -(m-Y_{\dot{v}})\dot{\psi}s_\psi c_\psi & -C_{22} & 0 & C_{24} \\ 0 & 0 & 0 & 0 \\ C_{41} & C_{42} & 0 & 0 \end{bmatrix}, \tag{A.4}$$

where $C_{12} = (m-X_{\dot{u}})\dot{\psi}c_\psi$; $C_{14} = (m-Y_{\dot{v}})(\dot{y}c_\psi - \dot{x}s_\psi)$; $C_{22} = (m-Y_{\dot{v}})\dot{\psi}s_\psi$; $C_{24} = (m-X_{\dot{u}})(\dot{x}c_\psi + \dot{y}s_\psi)$; $C_{41} = c_\psi(m-Y_{\dot{v}})(\dot{y}c_\psi - \dot{x}s_\psi) + s_\psi(m-X_{\dot{u}})(\dot{x}c_\psi + \dot{y}s_\psi)$ and $C_{42} = s_\psi(m-Y_{\dot{v}})(\dot{y}c_\psi - \dot{x}s_\psi) - c_\psi(m-X_{\dot{u}})(\dot{x}c_\psi + \dot{y}s_\psi)$. Rewriting the damping matrix in the inertial system, we have to

$$\bar{D}(\dot{\bar{\eta}}) = \begin{bmatrix} d_{11} & d_{12} & 0 & 0 \\ d_{21} & d_{22} & 0 & 0 \\ 0 & 0 & -Z_W - Z_{w_{|w|}}|\dot{z}| & 0 \\ 0 & 0 & 0 & -N_r - N_{r_{|r|}}|\dot{\psi}| \end{bmatrix}, \tag{A.5}$$

where

$$\begin{aligned} d_{11} &= -c_\psi(X_u + X_{u_{|u|}}|\dot{x}c_\psi + \dot{y}s_\psi|), \\ d_{12} &= -s_\psi(X_u + X_{u_{|u|}}|\dot{x}c_\psi + \dot{y}s_\psi|), \\ d_{21} &= s_\psi(Y_v + Y_{v_{|v|}}|\dot{y}c_\psi - \dot{x}s_\psi|), \\ d_{22} &= -c_\psi(Y_v + Y_{v_{|v|}}|\dot{y}c_\psi - \dot{x}s_\psi|). \end{aligned} \tag{A.6}$$

The BlueROV2 consists of 6 thrusters which allows the vehicle to move freely in four degrees of freedom, the thrusters of 1 to 4 generate lateral movements, forward and reverse, in addition to generating the rotational movement in yaw. The thrusters 5 and 6 is are used to generate immersion and emersion. The configuration of the thrusters is shown in Fig. 17. The vector of forces and torques $\bar{\tau}$ is given as follows:

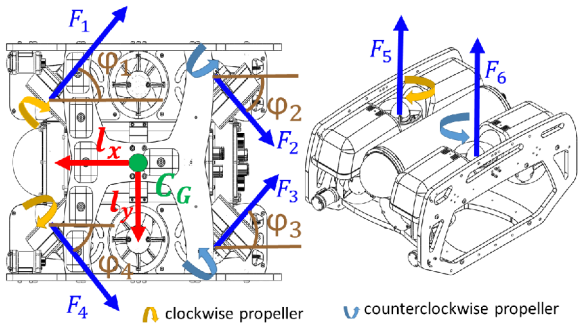

Fig. 17. The thrusters 5 and 6 are used to submerge and emerge. Thrusters 1 to 4 are used for the advance-recoil motion and the rotation movement in yaw.

$$\bar{\tau} = \begin{bmatrix} -\sum_{i=1}^{4} F_i c_{\varphi_i} \\ \sum_{i=1}^{4}(-1)^i F_i s_{\varphi_i} \\ -F_5 - F_6 \\ \sum_{i=1}^{4}(l_x F_i s_{\varphi_i} + l_y F_i c_{\varphi_i}) sign(i-2.5) \end{bmatrix}, \tag{A.7}$$

where l_y, l_x is the distance between the center of gravity of the vehicle to the thrusters on the axis y and x, respectively.

In order to simplify the notation, we rewrite equation (A.1) as follows:

$$\ddot{\bar{\eta}} = \bar{C}_\eta(\bar{\eta},\dot{\bar{\eta}})\dot{\bar{\eta}} + \bar{D}_\eta(\bar{\eta},\dot{\bar{\eta}})\dot{\bar{\eta}} + \bar{g}_\eta(\bar{\eta}) + \bar{\tau}_\eta, \tag{A.8}$$

where

$$\begin{aligned} \bar{C}_\eta(\bar{\eta},\dot{\bar{\eta}}) &= -\bar{M}^{-1}(\bar{\eta})\bar{C}(\bar{\eta},\dot{\bar{\eta}}), \\ \bar{D}_\eta(\bar{\eta},\dot{\bar{\eta}}) &= -\bar{M}^{-1}(\bar{\eta})\bar{D}(\bar{\eta},\dot{\bar{\eta}}), \\ \bar{g}_\eta(\bar{\eta}) &= -\bar{M}^{-1}(\bar{\eta})\bar{g}(\bar{\eta}), \\ \bar{\tau}_\eta &= \bar{M}^{-1}(\bar{\eta})\bar{\tau}. \end{aligned} \tag{A.9}$$

From (A.8), we obtain the following expressions for the dynamics of the UUV

$$\begin{aligned} \ddot{x} = &\, s_\psi \frac{Y - (Y_v + Y_{v|v|}|\dot{y}c_\psi - \dot{x}s_\psi|)(\dot{y}c_\psi - \dot{x}s_\psi)}{Y_{\dot{v}} - m} \\ &+ s_\psi \frac{\dot{\psi}(X_{\dot{u}} - m)(\dot{x}c_\psi + \dot{y}s_\psi)}{Y_{\dot{v}} - m} \\ &- \dot{\psi}(s_\psi + c_\psi)(\dot{x}c_\psi + \dot{y}s_\psi) \\ &+ c_\psi \frac{(X_u + X_{u_{|u|}}|\dot{x}c_\psi + \dot{y}s_\psi|)(\dot{x}c_\psi + \dot{y}s_\psi) - X}{X_{\dot{u}} - m} \\ &+ c_\psi \frac{\dot{\psi}(Y_{\dot{v}} - m)(\dot{y}c_\psi - \dot{x}s_\psi)}{X_{\dot{u}} - m}, \\ \ddot{y} = &\, \dot{\psi}c_\psi(\dot{x}c_\psi + \dot{y}s_\psi) - \dot{\psi}s_\psi(\dot{y}c_\psi - \dot{x}s_\psi) \\ &- c_\psi \frac{Y - (Y_v + Y_{v|v|}|\dot{y}c_\psi - \dot{x}s_\psi|)(\dot{y}c_\psi - \dot{x}s_\psi)}{Y_{\dot{v}} - m} \end{aligned}$$

$$
\begin{aligned}
&- c_\psi \frac{\dot{\psi}(X_{\dot{u}} - m)(\dot{x}c_\psi + \dot{y}s_\psi)}{Y_{\dot{v}} - m} \\
&+ s_\psi \frac{(X_u + X_{u_{|u|}}|\dot{x}c_\psi + \dot{y}s_\psi|)(\dot{x}c_\psi + \dot{y}s_\psi)}{X_{\dot{u}} - m} \\
&+ s_\psi \frac{-X + \dot{\psi}(Y_{\dot{v}} - m)(\dot{y}c_\psi - \dot{x}s_\psi)}{X_{\dot{u}} - m}, \qquad \text{(A.10)} \\
\ddot{z} &= \frac{B - W + Z_w\dot{z} + Z_{w_{|w|}}\dot{z}|\dot{z}|}{Z_{\dot{w}} - m} - \frac{1}{Z_{\dot{w}} - m}Z, \\
\ddot{\psi} &= -\frac{(X_{\dot{u}} - m)(\dot{x}c_\psi + \dot{y}s_\psi)(\dot{y}c_\psi - \dot{x}s_\psi)}{I_{zz} - N_{\dot{r}}} \\
&+ \frac{(Y_{\dot{v}} - m)(\dot{x}c_\psi + \dot{y}s_\psi)(\dot{y}c_\psi - \dot{x}s_\psi)}{I_{zz} - N_{\dot{r}}} \\
&- \frac{\dot{\psi}(N_r + N_{r_{|r|}}|\dot{\psi}|)}{I_{zz} - N_{\dot{r}}} + \frac{1}{I_{zz} - N_{\dot{r}}}N.
\end{aligned}
$$

In this work, we assume that the angle ψ is first controlled at zero ($\psi = 0$, $\dot{\psi} = 0$). Under this assumption, (A.10) is rewritten as follows:

$$
\begin{aligned}
\ddot{x} &= \frac{X_u\dot{x} + X_{u|u|}\dot{x}|\dot{x}|}{X_{\dot{u}} - m} - \frac{1}{X_{\dot{u}} - m}X, \\
\ddot{y} &= \frac{Y_v\dot{y} + Y_{v|v|}\dot{y}|\dot{y}|}{Y_{\dot{v}} - m} - \frac{1}{Y_{\dot{v}} - m}Y, \\
\ddot{z} &= \frac{B - W + Z_w\dot{z} + Z_{w_{|w|}}\dot{z}|\dot{z}|}{Z_{\dot{w}} - m} - \frac{1}{Z_{\dot{w}} + m}Z. \qquad \text{(A.11)}
\end{aligned}
$$

Finally, for the development of the control law, the following terms of (A.11) were defined as

$$
\begin{aligned}
f_x &= \frac{X_u\dot{x} + X_{u|u|}\dot{x}|\dot{x}|}{X_{\dot{u}} - m}, \\
f_y &= \frac{Y_v\dot{y} + Y_{v|v|}\dot{y}|\dot{y}|}{Y_{\dot{v}} - m}, \\
f_z &= \frac{B - W + Z_w\dot{z} + Z_{w|w|}\dot{z}|\dot{z}|}{Z_{\dot{w}} - m}, \\
f_\psi &= -\frac{(X_{\dot{u}} - m)(\dot{x}c_\psi + \dot{y}s_\psi)(\dot{y}c_\psi - \dot{x}s_\psi)}{I_{zz} - N_{\dot{r}}} \\
&+ \frac{(Y_{\dot{v}} - m)(\dot{x}c_\psi + \dot{y}s_\psi)(\dot{y}c_\psi - \dot{x}s_\psi)}{I_{zz} - N_{\dot{r}}} \\
&- \frac{\dot{\psi}(N_r + N_{r_{|r|}}|\dot{\psi}|)}{I_{zz} - N_{\dot{r}}}, \\
g_x &= -\frac{1}{X_{\dot{u}} - m}, \\
g_y &= -\frac{1}{Y_{\dot{v}} - m}, \\
g_z &= -\frac{1}{Z_{\dot{w}} + m}, \\
g_\psi &= \frac{1}{I_{zz} - N_{\dot{r}}}. \qquad \text{(A.12)}
\end{aligned}
$$

REFERENCES

[1] W. Naeem, R. Sutton, S. Ahmad, and R. Burns, "A review of guidance laws applicable to unmanned underwater vehicles," *The Journal of Navigation*, vol. 56, no. 1, pp. 15-29, 2003.

[2] S. M. Veres, L. Molnar, N. K. Lincoln, and C. P. Morice, "Autonomous vehicle control systems—a review of decision making," *Proceedings of the Institution of Mechanical Engineers, Part I: Journal of Systems and Control Engineering*, vol. 225, no. 2, pp. 155-195, 2011.

[3] J. Melo and A. Matos, "Survey on advances on terrain based navigation for autonomous underwater vehicles," *Ocean Engineering*, vol. 139, pp. 250-264, 2017.

[4] J. Partan, J. Kurose, and B. N. Levine, "A survey of practical issues in underwater networks," *ACM SIGMOBILE Mobile Computing and Communications Review*, vol. 11, no. 4, pp. 23-33, 2007.

[5] L. Stutters, H. Liu, C. Tiltman, and D. J. Brown, "Navigation technologies for autonomous underwater vehicles," *IEEE Transactions on Systems, Man, and Cybernetics, Part C (Applications and Reviews)*, vol. 38, no. 4, pp. 581-589, 2008.

[6] J. Lee, M. Roh, J. Lee, and D. Lee, "Clonal selection algorithms for 6-dof PID control of autonomous underwater vehicles," *Proc. of International Conference on Artificial Immune Systems*, Springer, pp. 182-190, 2007.

[7] J. Bak, H.-N. Nguyen, S. Park, D. Lee, T. Seo, S. Jin, and J. Kim, "Positioning control of an underwater robot with tilting thrusters via decomposition of thrust vector," *International Journal of Control, Automation and Systems*, vol. 15, no. 5, pp. 2283-2291, 2017.

[8] A. Zamora, A. Manzanilla, M. Garcia, R. Lozano, S. Salazar, and F. Muñoz, "Depth control of an underwater vehicle using robust pd controller: real-time experiments," *Proc. of IEEE OES Autonomous Underwater Vehicle Symposium*, pp. 1-6, 2018.

[9] S. Pang, J. Wang, J. Liu, and H. Yi, "Three-dimensional leader-follower formation control of multiple autonomous underwater vehicles based on line-of-sight measurements using the backstepping method," *Proceedings of the Institution of Mechanical Engineers, Part I: Journal of Systems and Control Engineering*, vol. 232, no. 7, pp. 819-829, 2018.

[10] I.-L. Borlaug, K. Y. Pettersen, and J. T. Gravdahl, "Trajectory tracking for an articulated intervention AUV using a super-twisting algorithm in 6 dof," *IFAC-PapersOnLine*, vol. 51, no. 29, pp. 311-316, 2018.

[11] C. H. F. dos Santos, M. U. Cildoz, M. H. Terra, and E. R. D. Pieri, "Backstepping sliding mode control with functional tuning based on an instantaneous power approach applied to an underwater vehicle," *International Journal of Systems Science*, vol. 49, no. 4, pp. 859-867, 2018.

[12] E. Anderlini, G. G. Parker, and G. Thomas, "Control of a rov carrying an object," *Ocean Engineering*, vol. 165, pp. 307-318, 2018.

[13] S. Li and Y. Peng, "Neural network-based sliding mode variable structure control for mars entry," *Proceedings of the Institution of Mechanical Engineers, Part G: Journal of Aerospace Engineering*, vol. 226, no. 11, pp. 1373-1386, 2012.

[14] Z. Chu, X. Xiang, D. Zhu, C. Luo, and D. Xie, "Adaptive fuzzy sliding mode diving control for autonomous underwater vehicle with input constraint," *International Journal of Fuzzy Systems*, vol. 20, no. 5, pp. 1460-1469, 2018.

[15] V. I. Utkin, "Sliding mode control design principles and applications to electric drives," *IEEE Transactions on Industrial Electronics*, vol. 40, no. 1, pp. 23-36, 1993.

[16] A. Levant, "Chattering analysis," *IEEE Transactions on Automatic Control*, vol. 55, no. 6, pp. 1380-1389, 2010.

[17] S. Yu, X. Yu, B. Shirinzadeh, and Z. Man, "Continuous finite-time control for robotic manipulators with terminal sliding mode," *Automatica*, vol. 41, no. 11, pp. 1957-1964, 2005.

[18] J. A. Moreno and M. Osorio, "Strict lyapunov functions for the super-twisting algorithm," *IEEE Transactions on Automatic Control*, vol. 57, no. 4, pp. 1035-1040, 2012.

[19] L. Derafa, A. Benallegue, and L. Fridman, "Super twisting control algorithm for the attitude tracking of a four rotors uav," *Journal of the Franklin Institute*, vol. 349, no. 2, pp. 685-699, 2012.

[20] A. Chalanga, S. Kamal, L. M. Fridman, B. Bandyopadhyay, and J. A. Moreno, "Implementation of super-twisting control: Super-twisting and higher order sliding-mode observer-based approaches," *IEEE Transactions on Industrial Electronics*, vol. 63, no. 6, pp. 3677-3685, 2016.

[21] S. Mobayen, F. Tchier, and L. Ragoub, "Design of an adaptive tracker for n-link rigid robotic manipulators based on super-twisting global nonlinear sliding mode control," *International Journal of Systems Science*, vol. 48, no. 9, pp. 1990-2002, 2017.

[22] L. Yang and J. Yang, "Nonsingular fast terminal sliding-mode control for nonlinear dynamical systems," *International Journal of Robust and Nonlinear Control*, vol. 21, no. 16, pp. 1865-1879, 2011.

[23] Y.-Z. Sheng, J. Geng, X.-D. Liu, and L. Wang, "Nonsingular finite-time second order sliding mode attitude control for reentry vehicle," *International Journal of Control, Automation and Systems*, vol. 13, no. 4, pp. 853-866, 2015.

[24] H. Wang, L. Shi, Z. Man, J. Zheng, S. Li, M. Yu, C. Jiang, H. Kong, and Z. Cao, "Continuous fast nonsingular terminal sliding mode control of automotive electronic throttle systems using finite-time exact observer," *IEEE Transactions on Industrial Electronics*, vol. 65, no. 9, pp. 7160-7172, 2018.

[25] Y. Wang, L. Gu, M. Gao, X. Jia, J. Zhou, J. Liu, and D. Zhou, "Depth control of remotely operated vehicles using nonsingular fast terminal sliding mode control method," *Proc. of OCEANS*, San Diego, pp. 1-6, 2013.

[26] Z. Yan, H. Yu, W. Zhang, B. Li, and J. Zhou, "Globally finite-time stable tracking control of underactuated UUVs," *Ocean Engineering*, vol. 107, pp. 132-146, 2015.

[27] T. Elmokadem, M. Zribi, and K. Youcef-Toumi, "Terminal sliding mode control for the trajectory tracking of underactuated autonomous underwater vehicles," *Ocean Engineering*, vol. 129, pp. 613-625, 2017.

[28] P. S. Londhe, D. D. Dhadekar, B. M. Patre, and L. M. Waghmare, "Non-singular terminal sliding mode control for robust trajectory tracking control of an autonomous underwater vehicle," *Proc. of the Indian Control Conference (ICC)*, pp. 443-449, 2017.

[29] Y. B. Shtessel, J. A. Moreno, F. Plestan, L. M. Fridman, and A. S. Poznyak, "Super-twisting adaptive sliding mode control: A lyapunov design," *Proc. of 49th IEEE Conference on Decision and Control (CDC)*, pp. 5109-5113, 2010.

[30] J. A. González, A. Barreiro, and S. Dormido, "A practical approach to adaptive sliding mode control," *International Journal of Control, Automation and Systems*, vol. 17, no. 7, pp. 2452-2461, 2019.

[31] Y. Shtessel, M. Taleb, and F. Plestan, "A novel adaptive-gain supertwisting sliding mode controller: Methodology and application," *Automatica*, vol. 48, no. 5, pp. 759-769, 2012.

[32] J. Guerrero, J. Torres, V. Creuze, and A. Chemori, "Trajectory tracking for autonomous underwater vehicle: An adaptive approach," *Ocean Engineering*, vol. 172, pp. 511-522, 2019.

[33] C.-S. Jeong, J.-S. Kim, and S.-I. Han, "Tracking error constrained super-twisting sliding mode control for robotic systems," *International Journal of Control, Automation and Systems*, vol. 16, no. 2, pp. 804-814, 2018.

[34] S. Mobayen, "Adaptive global terminal sliding mode control scheme with improved dynamic surface for uncertain nonlinear systems," *International Journal of Control, Automation and Systems*, vol. 16, no. 4, pp. 1692-1700, 2018.

[35] Z. Yan, M. Wang, and J. Xu, "Robust adaptive sliding mode control of underactuated autonomous underwater vehicles with uncertain dynamics," *Ocean Engineering*, vol. 173, pp. 802-809, 2019.

[36] L. Qiao and W. Zhang, "Double-loop integral terminal sliding mode tracking control for uuvs with adaptive dynamic compensation of uncertainties and disturbances," *IEEE Journal of Oceanic Engineering*, vol. 44, no. 1, pp. 29-53, 2019.

[37] L. Qiao and W. Zhang, "Adaptive second-order fast nonsingular terminal sliding mode tracking control for fully actuated autonomous underwater vehicles," *IEEE Journal of Oceanic Engineering*, vol. 44, no. 2, pp. 363-385, 2018.

[38] L. Qiao and W. Zhang, "Adaptive non-singular integral terminal sliding mode tracking control for autonomous underwater vehicles," *IET Control Theory Applications*, vol. 11, no. 8, pp. 1293-1306, 2017.

[39] S. H. Sname, "Nomenclature for treating the motion of a submerged body through a fluid," *American Towing Tank Conference*, 1950.

[40] T. I. Fossen, *Handbook of Marine Craft Hydrodynamics and Motion Control*, John Wiley & Sons, 2011.

[41] Z. Zhu, Y. Xia, and M. Fu, "Attitude stabilization of rigid spacecraft with finite-time convergence," *International Journal of Robust and Nonlinear Control*, vol. 21, no. 6, pp. 686-702, 2011.

[42] Y. Wang, J. Chen, F. Yan, K. Zhu, and B. Chen, "Adaptive super-twisting fractional-order nonsingular terminal sliding mode control of cable-driven manipulators," *ISA Transactions*, vol. 86, pp. 163-180, 2019.